

A Study of Charging Behaviors in Organic Semiconductors using Optical Trapping

by  
Graham M. Founds

A PROJECT

submitted to

Oregon State University

in partial fulfillment of  
the requirements for the  
degree of

Baccalaureate of Science in Physics

Presented June 6, 2017  
Commencement June 2017

## **Abstract**

We measure the charging and discharging of two organic materials, PCBM and ADT-TES-F. These materials are studied through the noncontact method of particle trapping known as Optical Tweezers, where an IR laser is used to constrain the motion of a coated or noncoated silica sphere while its positional data is recorded. The surface charge of the sphere is calculated via an induced driving electric field. We focus on the governing experimental parameters of the electric field frequency, electric field intensity, and the power of a PL inducing excitation laser. These parameters directly affect the surface charge density of a silica sphere trapped in an optical tweezer by altering the environment in which surface charge is induced. These parameters also govern how charges move in the valence and conduction bands. In previous research the electric field frequency and amplitude were set to values that did not yield a reliable surface charge. The electric field applied to the coated or noncoated spheres must exhibit a driving frequency greater than 300 Hz in contrast to the previously used 100-110 Hz. The electric field amplitude must be greater than 2000 V/m to produce reliable surface charge measurement in contrast to the previously used 500-1000 V/m field. The power of that excitation laser has no effect on the surface charge density of plain silica spheres regardless of the presence of PCBM. Knowing the required parameters removes the need to have a calibration factor applied to future experiments conducted with spheres coated with the photo luminescent ADT-TES-F.

## **Keywords**

Organic Semiconductors, Optical Trapping, Optical Tweezers, ADT-TES-F, PCBM, Charge Transfer, Charging Behavior, Microspheres.

# Table of Contents

List of Figures	5
Chapter 1: Introduction	7
1.1 Motivation.....	7
1.2 Objectives.....	8
1.3 Optical Trapping.....	10
1.3.1 Optical Tweezers.....	10
1.3.2 Optical Trapping of Microspheres.....	11
1.4 Organic Semiconductors.....	12
1.4.1 ADT-TES-F.....	12
1.4.2 PCBM.....	14
1.5 Charge Measurement.....	15
1.5.1 Surface Charge Measurement of Microspheres.....	15
1.6 Data Analysis.....	15
1.6.1 Trap Stiffness.....	16
1.6.2 Surface Charge.....	17
Chapter 2: Methods	20
2.1 Overview.....	20
2.2 Sample Preparation.....	23
2.2.1 Silica and Water.....	23
2.2.2 Silica and PCBM in Water.....	24
2.2.3 ADT-TES-F Coated Silica with PCBM in Water.....	24
2.3 Sample Holder Preparation.....	26
2.3.1 Simple.....	26
2.3.2 Complex.....	27
2.4 Experimental Set-up.....	30
2.5 Data Collection.....	33

2.5.1	Trap stiffness Measurements.....	33
2.5.2	Control Charge Measurements.....	33
2.5.3	Charge as a Function of Driving Field Frequency.....	36
2.5.4	Charge as a Function of Driving Field Intensity.....	36
2.5.5	Charge as a Function of Excitation Laser Intensity.....	36
<b>Chapter 3: Results and Discussion</b>		<b>38</b>
3.1	Trap Stiffness.....	39
3.1.1	Trap Stiffness as a Function of Trapping Laser Power.....	39
3.2	Surface Charge of Microsphere.....	40
3.2.1	Silica in Water.....	40
3.2.2	Silica in Water with PCBM.....	45
<b>Chapter 4: Conclusions</b>		<b>49</b>
<b>Acknowledgements</b>		<b>50</b>
<b>References</b>		<b>51</b>

# List of Figures

## Chapter 1: Introduction

1.1	Samsung's new flexible AMOLD OLED display.....	7
1.2	Organic semiconductors are printed into thin films.....	8
1.3	Forces experienced by microsphere during optical trapping.....	11
1.4	Sphere resting below focal point of trapping laser.....	12
1.5	Molecular structure of base Anthradithiophene (ADT).....	13
1.6	Molecular structure of the aromatic fullerene (PCBM).....	14
1.7	Sample of data analysis results from the MATLAB.....	16

## Chapter 2: Methods

2.1	Basic outline of experiments conducted.....	21
2.2	Top view of simple sample holder.....	26
2.3	Side view of simple sample holder.....	26
2.4	Top view of the complex sample holder.....	27
2.5	Side view of the complex sample holder.....	28
2.6	Locations for injection holes.....	28
2.7	Interaction between microsphere and aluminum electrodes.....	29
2.8	Optical trapping set-up.....	30
2.9	Coated micro-sphere trapped in optical tweezer.....	34
2.10	Coated microsphere reacting to the excitation laser.....	35

## Chapter 3: Results and Discussion

3.1	Trapping Laser Power vs Trapping Stiffness.....	39
3.2	Silica + Water: Surface Charge Density vs Driving Field Frequency.....	40
3.3	Silica + Water: Surface Charge Density vs Excitation Laser Power.....	42
3.4	Silica + Water: Surface Charge Density vs Electric Field Intensity.....	43
3.5	Silica + Water + PCBM: Surface Charge Density vs Driving Field Frequency.....	45
3.6	Silica + Water + PCBM: Surface Charge Density vs Excitation Laser Intensity.....	46
3.7	Silica + Water + PCBM: Surface Charge Density vs Electric Field Intensity.....	47

# Chapter 1: Introduction

## 1.1 Motivation

Organic semiconductors are of considerable interest in the opto-electronic field. They boast a diverse spectrum of applications due to their tunable properties, efficiency, ease of production, low cost, and literal “flexibility” when grown into a thin film. In a society that glorifies technological progression and ingenuity, organic semiconductors have broadened the possibilities for solar cells, transistors, and malleable electronics. Many of us experience these advances in organic technology on a daily basis. Organic semiconductors are used in a wide variety of technology ranging from smartphones and flexible displays to artistic tints and stains.



Figure 1.1: Patented concept and Prototype for Samsung’s new flexible AMOLED OLED display. Flexible displays are created by “printing” organic semiconductors onto a substrate between cathode and anode layers [1].

In the production of smart phones a common screen type is called AMOLED, an acronym for Active-matrix organic light-emitting diode. These displays have become extremely popular due to their ability to allow curvature and flexibility in electronics. The popular cell phone manufacturer “Samsung” recently secured a patent for a smartphone with a flexible AMOLED

display, taking the field of applied organics a step further. Their phone release, projected for 2017-2018, will have a flexible AMOLED display, see Figure 1.1. These displays consist of organic light-emitting diodes (OLEDs) in series with Organic Thin-Film Transistors (OTFTs) [2]. The OTFTs control the amount of current

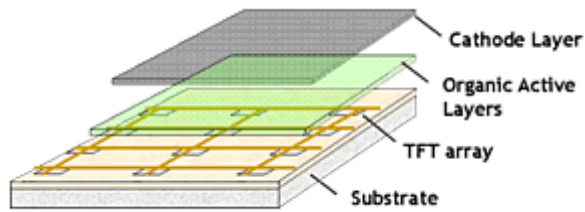


Figure 1.2: Organic semiconductors are printed into thin films for the “organic active layers”. These layers are then sandwiched between the TFT arrays, held on top of a substrate, and a cathode layer.

flowing through the OLEDs, dictating the brightness of the OLEDs and the AMOLED display, see Figure 1.2. Each pixel of an AMOLED display is associated with at least two separate OTFTs and an OLED panel: one OTFT to monitor the charging and discharging of a storage capacitor and the second to serve as a voltage source [3]. OLEDs may be the brightest star

of the organic optoelectronics field, but OTFT technology is crucial in the fabrication of AMOLED displays and improved image quality in LCDs. My work has been focused on organics that are most ideal for the manufacturing of OTFTs and organic solar cells, focusing on the organic semiconductors ADT-TES-F and PCBM. Most opto-electronic applications of organics rely on donor-acceptor combinations. In solar cells, the acceptor provides low energy levels for electrons from the donor molecule to transfer to, encouraging charge separation. In OLEDs, electrons on the acceptor recombine with the holes on the donor resulting in light emission, such as the light of an AMOLED screen.

## 1.2 Objectives

I propose the development of a novel method of studying the charging and discharging characteristics of organic semiconductors using an optical trapping method known as optical tweezers. An important aspect of organic semiconductors is their ability to allow charge motion from a tightly bound energy level to the excited conduction band levels or the states of a neighboring molecule. The need for charge motion alludes to the importance of charging and discharge characteristics in organic semiconductors. To study these characteristics a non-invasive method is best employed for sensitivity and accuracy. By using a precision optical trapping set-up, optical tweezers, the charging and discharging dynamics of organic

semiconductors can be studied with accuracy and reliability. This non-contact method of study has the future ability to measure charging characteristics at an elementary charge resolution.

Charging behavior can be measured through the analysis of a particle coated in organic semiconductor while subject to optical trapping forces and an oscillatory electric field. These charge measurements yield data detailing the propensity of a semiconductor material to lose and gain charge to and from its immediate surroundings [4].

Optical Tweezing methods of measuring the charging behavior of organic semiconductors are based on the works of G. Seth Roberts and Tiffany A. Wood from the University of Bristol. The authors develop an ultrasensitive method for the measurement of the charge carried by a colloidal particle in a nonpolar suspension [5]. Roberts's research showed that the surface charge of a colloidal particle suspended in a non-polar environment could be measured through the analysis of the particles motion. We employ and expand upon Roberts's research to study organic semiconductors in a polar environment, such as water. The colloidal particle, represented by a microsphere, is coated in a donor organic molecule or used as a plain sphere and subject to an optical trap and driving electric field. The positional data is then used to calculate the surface charge of the sphere, thus studying the charging behaviors of the coating or surrounding semiconductor.

We expand methods of optical tweezing to study organic donor-acceptor systems. Previously the distance between donor and acceptor molecules could not be controlled in organic experimentation. The electron donor materials are placed on a trapped sphere whilst leaving electron acceptor molecules suspended as macroscopic particulates in a solvent [6]. Through the development of this optical tweezing method, the

charging behaviors of organic donor-acceptor materials can be studied with elementary charge resolution at the nanoscale in a variety of dielectric environments.

## 1.3 Optical Trapping

### 1.3.1 Optical Tweezers.

Since their inception in the early 1970s, optical tweezers have been used to apply piconewton forces to microparticles [7]. The use of optical trapping methods such as optical tweezers were performed in an effort to gain insight into the characteristics and behaviors of particles suspended in an aqueous dielectric environment at the microscopic scale. Optical tweezers use light to manipulate microscopic particles using the radiation pressure from a focused Gaussian laser beam [8]. They are applied in a variety of fields of science ranging from atomic physics to medical science [7].

Many research communities use optical tweezers as a method of manipulating and controlling the position of a microparticle that is being studied. The wide spread use of optical tweezers as a form of manipulative position control is primarily due to the noninvasive nature of optical trapping. This aspect poses optical tweezers as a diverse and flexible tool for ultra-fine positioning, measurements, and control.

### 1.3.2 Optical Trapping of a Microsphere

Trapping microspheres is a common yet intriguing use for optical tweezers that can be performed to study the charge properties of a semiconductor, the dispersion forces of an aqueous dielectric, simulated trap stiffness of the optical trap, and the photo luminescence spectrum of an organic semiconductor.

In an optical tweezers set up, the trapped microsphere experiences restoring forces induced by the radiation pressure and scattering forces of the trapping Gaussian laser. The light from the trapping laser bends when passing through the refractive index barrier created between the external environment and the microsphere's surface. These restoring forces act like a spring force. The further from the laser focal point the sphere is, the stronger the restoring force it experiences, pulling it back to the focus. Figure 1.3 displays diagram of the fundamental forces involved in trapping a microsphere.

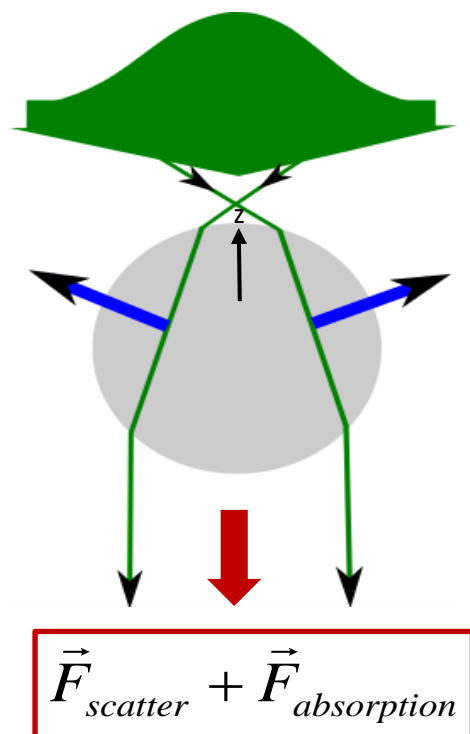


Figure 1.3: Forces experienced by microsphere during optical trapping. The trapping laser is represented by the Gaussian arrow pointing towards the sphere. The blue arrows show the direction of the force experienced by the sphere. Notice that the forces are in equilibrium at a rest location. The red arrow represents the scattering and absorption forces pushing the sphere downward from the focus of the laser. Image courtesy of the Organic Photonics and Electronics lab.

Due to the radiation pressure experienced by the sphere in the -z direction, displayed in Figure 1.3, the sphere comes to rest below the focus. The diagram of the trapped microsphere sitting just below the focus of the trapping laser is shown in Figure 1.4. The light rays **a** and **b**, in Figure 1.4, are focused through the objective lens. Without the sphere, they would combine at the true focus **f**. The change in index of refraction from the surrounding environment to the sphere, causes the light to slow and the focus drops. The new focus is shown where the slowed **a** and **b** connect. The center of the sphere is then pushed lower

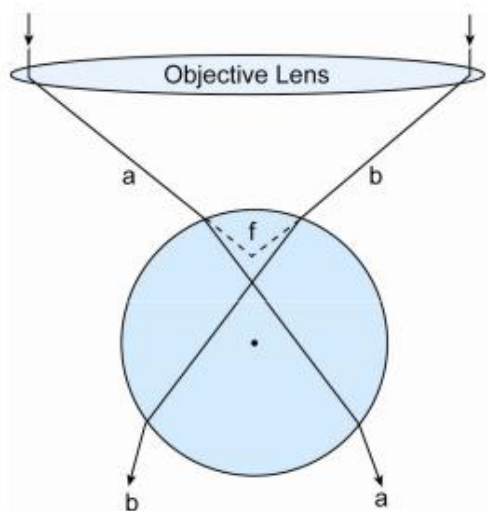


Figure 1.4: Sphere resting below focal point of trapping laser. Index of refraction causes beams a and b to slow, creating a new focus inside the spheres shell. Net downward force balances with environments buoyant force and causes sphere to reside below lasers true and adjusted focal point [8].

than the new “corrected” focus. This is due to the  $z$  components of the beams applying a net downward force which is then counteracted by the buoyant force of the surrounding environment. The sphere resides in an equilibrium of forces along the  $z$  axis and is held in place by the counteracting forces applied by the optically skewed light rays **a** and **b**, Figure 1.4.

## 1.4 Organic Semiconductors

The charging and discharging characteristics of two organic semiconductors are analyzed; one donor and one acceptor.

The chosen donor molecule is ADT-TES-F, a derivative of the base aromatic structure anthradithiophene (ADT). The Acceptor molecule used is phenyl- $C_{61}$ -butyric acid methyl ester (PCBM), a spherical aromatic or fullerene. These organics are used as an acceptor/donor pair in a polar environment to study their charging and discharging characteristics. ADT-TES-F and PCBM have been used previously in various organic devices such as solar cells and photo-transistors [9,10].

### 1.4.1 ADT-TES-F

Anthradithiophene (ADT) is the base aromatic structure, a donor molecule, chemically inclined to donate electrons to the surrounding environment or a nearby molecule; providing there are sufficient energy levels to encourage charge motion. To obtain ADT-TES-F, anthradithiophene is fluorinated and then functionalized with tri(ethylsilyl)ethynyl (TES) side groups [9]. ADT-TES-F exhibits 2D “brick-work” pi-stacking and forms crystalline films often utilized in thin-film transistors [9]. See the molecular structure of ADT and the functionalizing group TES in Figure 1.5 below. ADT-TES-F was chosen for its efficient vertical

pi-stacking, the exhibition of high charge carrier (hole) mobility's in thin-films, fast charge carrier photogeneration, high photoconductive gain, and relatively strong photoluminescence (PL) in solution-deposited thin films [11].

Organic molecules compete with the valance band and conduction band gaps held by modern inorganics, such as the material Silicon. Silicon is the most common semiconductor used today, it exhibits a 1.12 electron volt (ev) band gap, low manufacturing costs, ready abundance, and relative ease of use when doping with appropriate molecules.

ADT-TES-F comes close to the band gap dimensions of Silicon, at 2.3 eV [12]. However, a more present issue concerning organics is their narrow band widths, resulting in low charge mobility. Combining multiple molecules into molecular assemblies reduces the band gap and encouraging higher charge carrier mobility. ADT-TES-F's ability to be drop cast or "printed" onto a flexible substrate makes it drastically more diverse in application when compared to the rigid nature of

silicon and other conventional inorganic materials. Although there are some disadvantages, ADT-TES-F and its fellow organics have significant advantages over the common in-organic materials used as semiconductors.

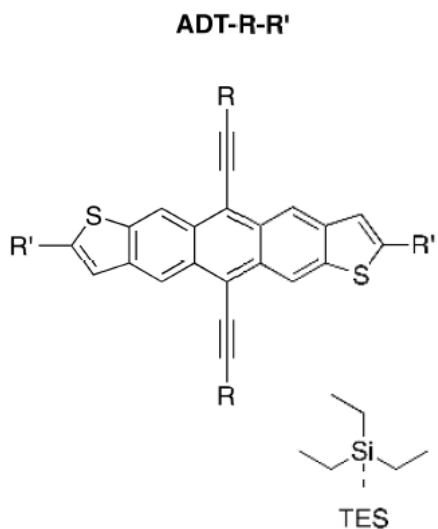


Figure 1.5: Molecular structure of base Anthradithiophene (ADT). ADT is an 'anti or syn isomer' structure, this is shown by the position of the Sulfur molecules on opposing or complimenting sides of the ADT structure. This isomer of ADT was chosen because anti-isomers showed higher field-effect mobility's [13]. As explained in the text, the R extensions are functionalized with the tri-(ethylsilyl)-ethynyl (TES) groups and then the molecule is fluorinated to fill the R' side groups with Fluorine molecules(F).

### 1.4.2 PCBM

Phenyl-C61-butyric acid methyl ester (PCBM) is a fullerene derivative of the C<sub>60</sub> buckyball that was first synthesized in the 1990s by Fred Wudl's group from the Institute for Polymers and Organic Solids and Departments of Chemistry and Materials at the University of California [14]. The molecular structure of PCBM can be seen in Figure 1.6 with brief explanation of its structure and active group. To date PCBM is one of the most widely studied active materials around the world for its use in bulk heterojunctions (BHJ), in which it acts as a universal acceptor [15]. BHJ refers to a molecular structure of donor and acceptor molecules that are indiscriminately mixed within a conglomeration.

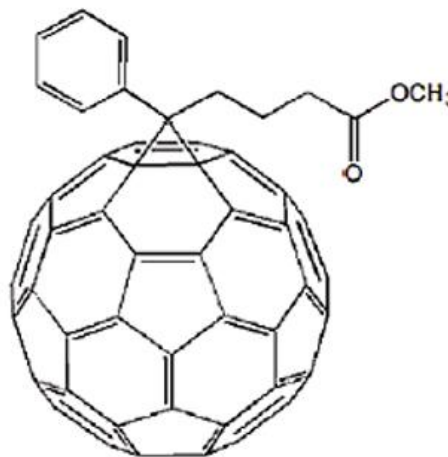


Figure 1.6: Molecular structure of the aromatic fullerene molecule Phenyl-C61-butyric acid methyl ester (PCBM), chemical formula C<sub>72</sub>H<sub>14</sub>O<sub>2</sub>. The base fullerene is augmented with a methoxy group (OCH<sub>3</sub>), a methyl group (CH<sub>3</sub>) bound to an oxygen (O). As affirmed by the Hammett equation developed by Louis Plack Hammett in 1937, methoxy is an electron donor group [14].

PCBM is an electron acceptor. It is chemically inclined to accept electrons from the surrounding environment or a nearby donor molecule due to its sufficiently low energy levels encouraging charge motion. PCBM is often used in solar cells or flexible electronics in conjunction with electron donor materials such as ADT-TES-F. PCBM is a more logical choice for an electron acceptor in comparison to other fullerene molecules because of its solubility. Its enhanced solubility allows PCBM to be easily processed into solutions of donor/acceptor mixes, a required property for printable organics that rely on donor/acceptor BHJ structures.

## 1.5 Charge Measurement

### 1.5.1 Surface Charge Measurement of Microspheres

When a microsphere is suspended in a dielectric environment in focus of an optical tweezer, if it is charged, an AC electric field can be applied to study the oscillating behavior of the microsphere. A charged sphere will experience an induced oscillation from the electric field as the surface charge interacts while a non-charged sphere will show no significant change in behavior in the presence of a driving field. To collect data, a quadrant photodetector (QPD) is coupled with a He-Ne detection laser being shone on the trapped microsphere. The QPD records the positional data of the microsphere by analyzing the fluctuations in the He-Ne laser. The particle's motion is analyzed to produce an approximate surface charge for the microsphere based on the extent to which the spheres motion was affected by the presence of the electric field.

## 1.6 Data Analysis

Data are analyzed using the theory and computational methods produced by G. Seth Roberts in his paper "Direct measurement of the effective charge in nonpolar suspension by optical tracking of single particles". Roberts et.al. developed an ultrasensitive method for the measurement of the charge carried by a colloidal particle in a nonpolar suspension [5]. This method was originally intended for use with a non-polar suspension, however there is no change in methodology when observing a particle in a polar suspension, such as water. Data is collected through the coupling of an optical trapping set-up and a LabVIEW code paired with a data acquisition unit or DAQ. The collected data is run through a MATLAB

program written by Rebecca Grollman, Doctoral Candidate at Oregon State University. An example of the data analysis output from the MATLAB code can be seen below in Figure 1.7.

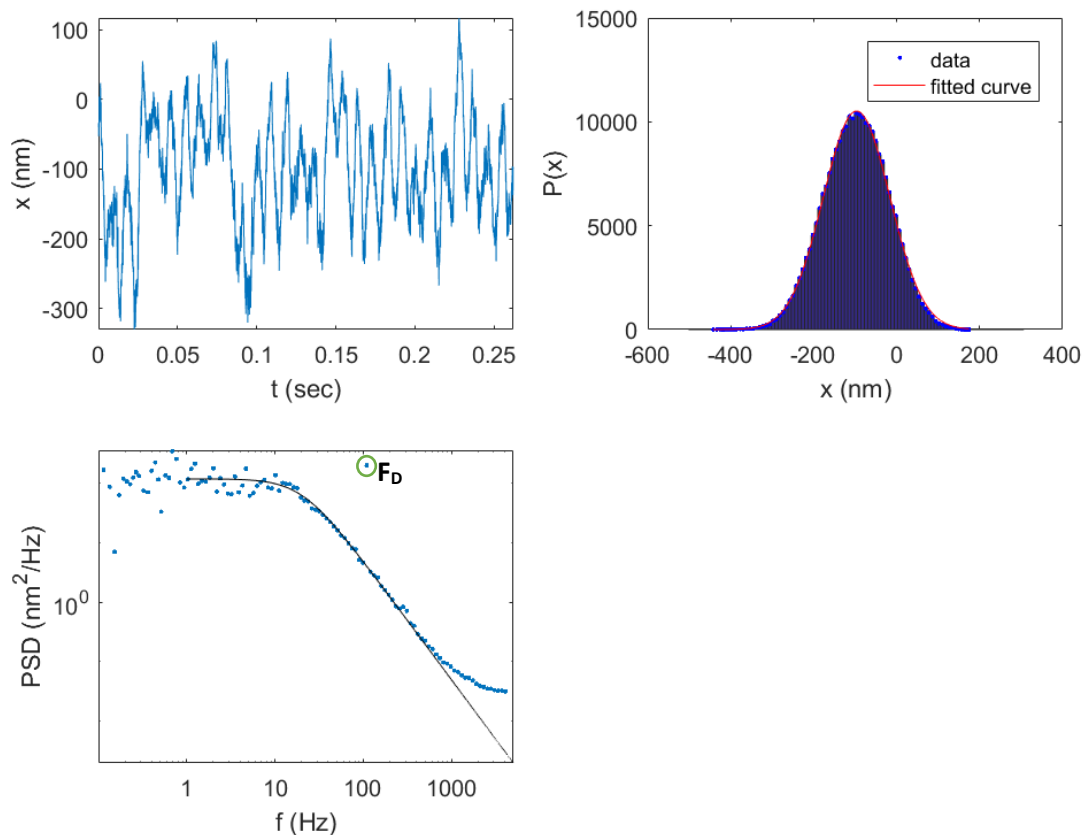


Figure 1.7: Sample of data analysis results from the MATLAB code provided by Rebecca Grollman. A) Simple position versus time plot of the trapped microsphere's motion within a short window of 300 milli-seconds. The applied oscillating electric field can be seen compounded with the standard Brownian motion of the microsphere in a fluid dielectric environment. B) A histogram of the positional data displayed in section A, fit with a Gaussian overlay which is visible as a red outline along the edges of the histogram. C) The frequency power spectrum of the sphere's motion. Displays the frequency spectrum of the spheres motion. The "corner" frequency used in the surface charge calculations lies on the inflection location where the data initiates a downward trend. The frequency used to drive the trapped microsphere is shown as the single elevated point around 100 Hz, labeled  $F_D$ .

### 1.6.1 Trap-stiffness

Trap stiffness refers to the simulated spring constant produced by the optical trapping of a microsphere in an optical tweezer. As described in the previous sections, a sphere held in an optical trap will feel a

restoring force pulling it back to the trap focus when it oscillates or drifts. The restoring force is found to be on the magnitude of piconewtons with units of piconewtons per micron and can be thought of as the  $k$  value for a spring, the stiffness. This value can be found to within 10-15% error [16].

The trap stiffness can be calculated through the analysis of the frequency power spectrum of position fluctuations [16], seen in image 1.7 section C. The fluctuations in position can be represented by equation (1).

$$|\tilde{x}(f)^2| = \frac{k_B T}{\pi^2 \beta (f_c^2 + f^2)} \quad (1)$$

In equation (1),  $f$  is the frequency,  $\beta$  is the drag coefficient of the microsphere in the aqueous environment and  $f_c$  is the corner frequency. The corner frequency is the observed inflection point seen on Figure 1.7 section C, where the spectrum exhibits a distinct downward corner. The corner frequency can be directly related to the trap stiffness (2):

$$f_c = \frac{k}{2\pi\beta} \quad (2)$$

These coupled equations produce the trap stiffness from the collected frequency spectrum data. The trap stiffness is expected to vary linearly with the magnitude of the trapping lasers power.

## 1.6.2 Surface Charge

In contrast to the simplicity of calculating the simulated trap stiffness of an optical tweezer, approximating the surface charge, and further, the surface charge density, is no simple task. As mentioned prior to 1.6.2, the methodology utilized is one of G. Seth Roberts et al [5]. Roberts's technique uses the positional resonance of a particle held in an optical trap and driven by an electric field. This field is produced by a supplied sinusoidal signal interacting between two electrodes in solution [5]. Before collected data is

analyzed for surface charge values and densities it must first be run through the aforementioned trap stiffness analysis code. The MATLAB program, used to analyze surface charge, utilizes results from the initial trap stiffness code along with other experimental parameters such as field intensity, electrode separation in the sample, and trapping laser power.

When an alternating electric field is applied to a trapped microsphere, an electric field dependent component is added to the spectrum seen in Figure 1.7 section C [16]. This component is added to Equation (1) resulting in:

$$|\tilde{x}(f)^2| = \frac{k_B T}{\pi^2 \beta (f_c^2 + f^2)} + \frac{k_B T \gamma^2}{2k} [\delta(f - f_{AC})] \quad (3)$$

In this equation,  $\gamma^2$  represents the ratio of the mean square periodic and Brownian forces and is calculated from the probability integral below:

$$P_{AC} = \int_{-\infty}^{\infty} |\tilde{x}(f)^2|_E df = \frac{k_B T}{k} \gamma^2 \quad (4)$$

In equation (4), the  $|\tilde{x}(f)^2|_E$  represents the power spectrum resulting from the applied electric field. Using the resulting  $\gamma^2$  value produced from equation (4) the  $Z_{eff}$  or the effective charge on the microsphere can be calculated by using the theory represented in G. Seth Roberts's paper. This is done with the equation:

$$e|Z_{eff}| = \frac{\gamma \beta}{E} \sqrt{\frac{2k_B T}{k} ((2\pi f_{AC})^2 + (k/\beta))} \quad (5)$$

where  $e$  represents the charge of an electron,  $f_{AC}$  is the frequency of the applied electric field and  $E$  is the amplitude of the electric field. With Eq.5.s the effective surface charge is calculated, it can then be divided by the surface area of a 1  $\mu\text{m}$  sphere to produce the approximate surface charge density.

## Chapter 2: Methods

### 2.1 Overview

Silica spheres with the diameter of  $0.99 \mu\text{m} \pm 0.01 \mu\text{m}$  are used to test the trap stiffness of an optical tweezing setup and the charge transfer behavior of organic semiconductors, specifically ADT-TES-F and PCBM, as mentioned in section 1.3. These microspheres are placed in a polar, aqueous suspension environment, such as Milli-Q filtered water. The sample solution is then placed into one of two different handmade sample holders, allowing the 800nm Ti-Sapphire optical trapping laser to constrain the spheres with little outside interference. Two types of sample holders are designed to test parameters concerning the optical trapping set up, these sample holders will be discussed in further detail in the later sections 2.3.1 and 2.3.2.

Sample types are individually prepared for each of the experimental pursuits; trap stiffness and electrical charging. A solution of Milli-Q filtered water and  $0.99 \pm 0.01 \mu\text{m}$  silica microspheres is used for testing the trap stiffness of the trapping laser. A second solution is used to test the charging and discharging behaviors of ADT-TES-F and PCBM. The ADT-TES-F solution is broken down into three sequentially tested solution bases; Silica spheres coated in ADT-TES-F in Milli-Q, non-coated silica spheres suspended in Milli-Q with chunks of PCBM in solution, and ADT-TES-F coated silica spheres suspended in Milli-Q with PCBM

in solution. Visual representations of the 4 different types of experimental samples can be seen in Figure 2.1. These samples will be covered in depth in section 2.2.

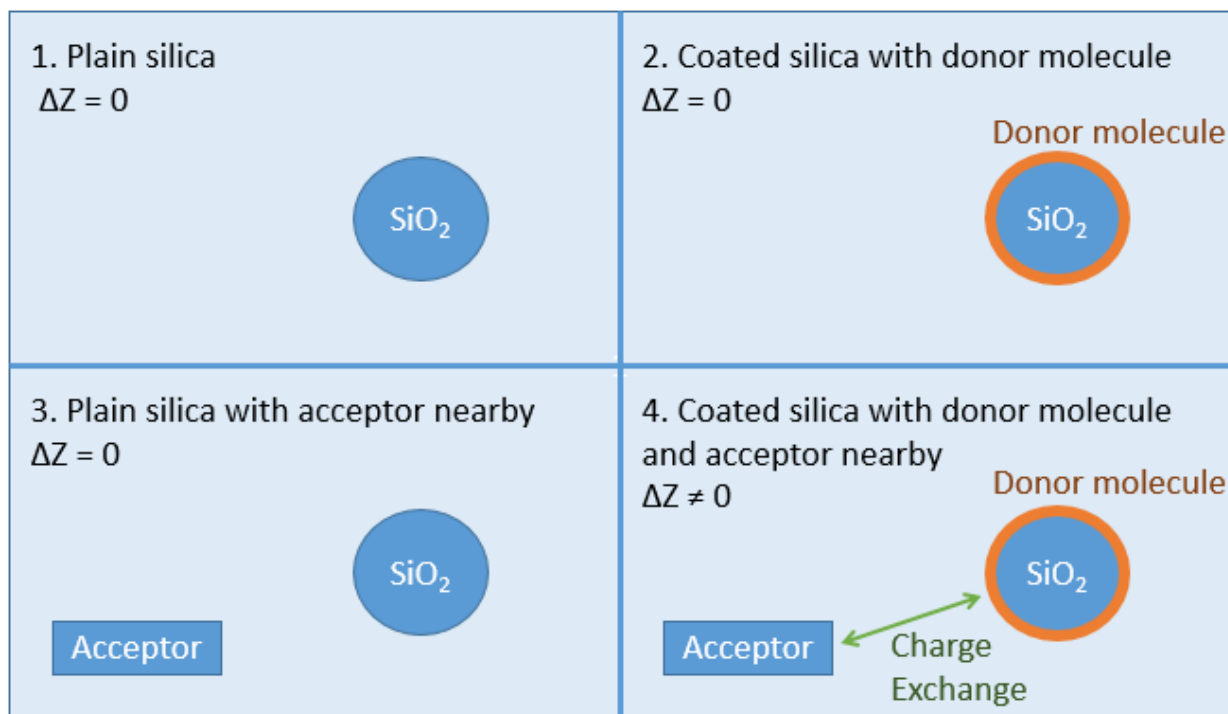


Figure 2.1: Basic outline of experiments conducted using each of the aforementioned solutions. 1) Plain silica is used to study trap stiffness and collect control values for surface charge of microsphere. 2) Silica coated in ADT-TES-F donor molecule tested for surface charging behaviors of donor molecule. 3) Plain silica with acceptor molecule in solution testing charging behavior between non-coated sphere and PCBM. 4) final experiment testing charging behaviors between donor ADT-TES-F and acceptor PCBM. Image courtesy of the Organic Photonics and Electronics lab.

The data collection methods for the trap stiffness and charging experiments are very similar with only a few changes to the experimental parameters and environment that the sphere/coated sphere is subject to. Both experiments rely on the positional data collected from a quadrant-photo-detector (QPD). The QPD reads the fluctuation in the intensity of a 2mW 633 nm He-Ne laser that is focused on the captured sphere. This process collects the positional data of the sphere as it experiences Brownian motion, or a combination of Brownian and driven motion, inside the optical trap. The motion of the sphere is constrained by the traps stiffness, which varies with the power of the Ti-Sapphire trapping laser. The

collected data is read and stored on a computer using a LabVIEW data collection program coupled with a DAQ panel. Using the collected positional data, the approximate trap stiffness is calculated, with MATLAB, for laser powers ranging from 3mW to 30mW.

The process of measuring charging behaviors is similar to that of the trap stiffness analysis, with the addition of an oscillating driving electric field applied through the sample solution. The trapping laser is held at a constant intensity, around 15 mW, and a coated or non-coated silica sphere is captured in the optical trap. The presence of a coating is dependent on the experiment being conducted, refer to Figure 2.1.

An electric field is applied to the sample with a chosen amplitude and frequency. A 532 nm excitation laser is used to observe photo-luminescence, or lack thereof. Photo-luminescence or PL is a form of light emission from matter after the absorption of photons. The observation of PL helps determine if a sphere is coated in an organic donor molecule, ADT-TES-F, or not. If a sphere is coated in ADT-TES-F, the 532nm laser should cause a glowing emission from the sphere which can be visualized with a CCD camera or measured with a spectrometer. To collect surface charge data, the HeNe laser is focused on the trapped coated sphere and the QPD reads the variance in its position within the trap. The data is collected by the same LabView program as before and fed to a MATLAB program that calculates the approximate surface charge of the coated microsphere.

## 2.2 Sample Preparation

Sample preparation follows very specific procedural guide lines to avoid sample contamination and possible exposure to harmful chemicals. Basic safety procedures are followed when using organic solutions such as toluene and acetone, both of which are used to clean and sterilize components during sample preparation and sample holder construction. Protective rubber gloves are always worn during sample preparation to ensure safety and sterility of sample solutions. All work performed with volatile chemicals is performed inside a ventilated fume hood, to reduce exposure to harmful fumes. If chemicals are used that are prone to evaporation, face-masks and eye protection are available in the sample preparation room.

For sample preparation, special Milli-Q filtered water is procured from Dr. Bo Sun's Collective Cell Biophysics lab in Oregon State's physics department. Milli-Q water has been specially distilled and fed through an ion exchange cartridge, which increases purity. Essentially Milli-Q water is distilled water that has been fed through special filters that ensure purity.

### 2.2.1 Silica in Milli-Q Water

The process of making each sample solution starts out with a 4 mL brown glass vial rinsed with toluene and distilled water inside the fume hood, to ensure that no contaminants remain in the container. Three pipets are available for use during sample preparation; 2-20 uL, 20-200 uL, and 200-1000 uL. Each pipet is rinsed with toluene and distilled water to ensure that contaminants are not injected into the solution. To mix the sample solution, 4 mL of Milli-Q filtered water are fed into the 4 mL vial using the 200-1000 uL pipet. Using the 2-20 uL pipet 2 uL of Thermo Scientific 0.99 +/- 0.01 um silica spheres are added to the 4 mL of Milli-Q water. The vial is sealed with the associated lid and wrapped with parafilm to ensure minimal exposure to contaminants. The filled vial is then submerged approximately 1 cm into the water bath of a

sonicator and sonicated for 10 minutes to help the silica spheres fully disperse in the aqueous solution. Once sonication is complete, the solution is labeled and stored in a desiccator until use for the experiment depicted in Figure 2.1 section 1.

### 2.2.2 Silica in Milli-Q Water with PCBM

Like the silica and Milli-Q sample solution, the addition of PCBM starts with a sterilized 4 mL vial, 4 mL of Milli-Q filtered water, and 2  $\mu$ L of the Thermo Scientific silica sphere solution. In the confines of the fume hood, an addition of 4.5  $\mu$ L of 1.05 mM PCBM and toluene solution introduces the acceptor molecule into the aqueous solution. The PCBM solution is cut from a 30 mM stock solution stored in the desiccator in the sample preparation room. The solution vial is then capped and sealed with parafilm, suspended 1 cm into the sonicator's water bath and sonicated for 20 minutes to ensure even distribution of the microspheres and the break down and distribution of the PCBM chunks. The solution vial is labeled and stored in the desiccator until use in the experiment depicted in Figure 2.1 section 3.

### 2.2.3 Silica Coated with ADT-TES-F in Milli-Q Water and with PCBM.

Coating silica spheres with ADT-TES-F is a tricky process and does not always work when creating sample solutions. Unfortunately, the solution must be fully developed and viewed under the optical tweezers set-up in order to see if the spheres were successfully coated.

Before starting the process of mixing the sample solution, the ADT-TES-F stock solution must be made from ADT-TES-F crystals and toluene. In a sterilized 4 mL brown glass vial, 4 mL of toluene and 72 mg of ADT-TES-F crystals are combined to create a 30 mM stock solution. The non-polar toluene dissolves the ADT-TES-F crystals, after sitting for 20 minutes in the isolation chamber the ADT-TES-F and toluene create

an evenly distributed solution, sonication is not needed in this process. The stock solution is available for use immediately after the 20 minute period.

In the fume hood, 50 mL of 30 mM ADT-TES-F stock is combined with 2 mL of silica spheres. The solution is sealed with a cap and parafilm then sonicated for 20 minutes to allow the spheres to dissociate into the ADT-TES-F solution. After sonication, 14  $\mu$ L of the ADT-TES-F and sphere solution are combined with 4 mL of Millit-Q water. The Milli-Q, ADT-TES-F, and silica sphere solution is allowed to sit in the isolation chamber overnight, giving the spheres more time to coat and distribute through the aqueous solution.

The following day the solution is sonicated for 20 minutes without the water bath being heated and 20 minutes with a heated water bath. At this point the sphere solution is ready to be used for the charging experiments, seen in Figure 2.1, section 2. One further step is taken to prepare the solution for the final experiment, Figure 2.1 section 4, 4.5  $\mu$ L of 1.05 mM PCBM solution is added to the ADT-TES-F and silica solution. This sample is then sonicated for 20 minutes to be made ready for use in experimental testing.

## 2.3 Sample Holder Preparation

Two unique sample holders are utilized in the testing of the sample solutions described in section 2.2. A simple sample holder design is used to study the behavior of the optical tweezers trap stiffness, “spring constant”, while a more complex design is used in the study of the charging and discharging behaviors of ADT-TES-F and PCBM in aqueous solution.

### 2.3.1 Trap Stiffness

The “simple” version of the sample holder is comprised of 3 base components; A glass microscope slide, a glass coverslip, and a custom made double sided adhesive square with a circular hole in the center. Top and side view diagrams can be seen in Figure 2.2 and 2.3 below.

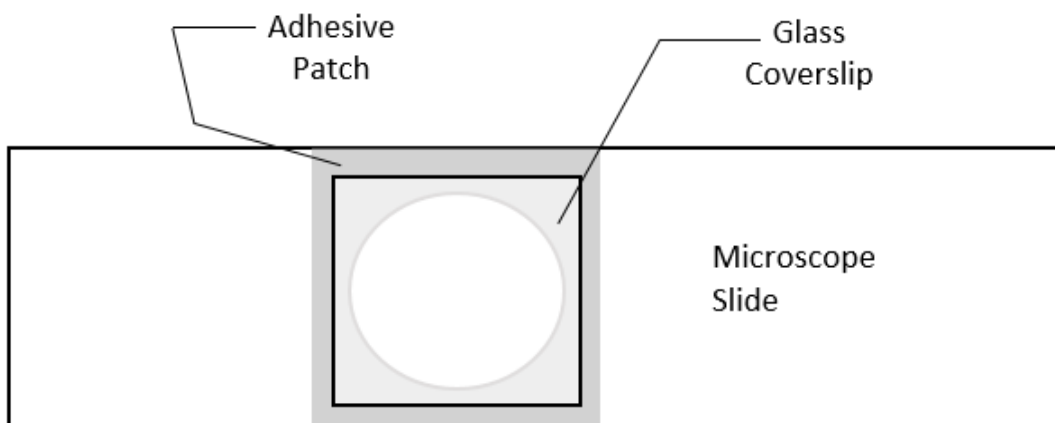


Figure 2.2: Top view of simple sample holder used in the experimental analysis of the optical tweezers trapping forces or "trap stiffness".

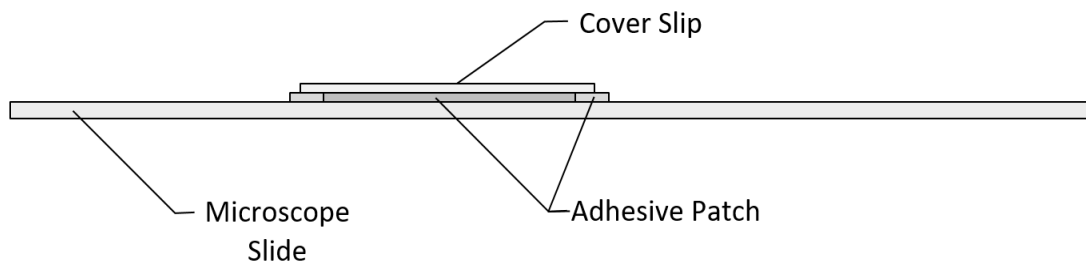


Figure 2.3: Side view of simple sample holder used in the experimental analysis of the optical tweezers trapping forces or "trap stiffness".

The microscope slide is cleaned with toluene in the fume hood and rinsed with DI water. This helps ensure that no outside contaminants enter the sample solution when the holder is being used. The freshly cleaned slide is placed on a sanitary matt outside the fume hood. The placement of the slide outside the hood is due to the presence of contaminating substances in the fume hood. The adhesive square is placed 1 cm off center on the glass slide, this allows for more mobile placement when inserting the sample holder into the optical tweezers set-up. 50  $\mu\text{L}$  of the chosen sample solution is placed in the center of the circular cut out of the adhesive square and the coverslip is placed on top of the adhesive so that all sides are fully secured, see Figure 2.2 for a descriptive diagram.

### 2.3.2 Charge Measurement

The experimental process to study the charging and discharging characteristics of ADT-TES-F and PCBM requires a more complicated sample holder that allows the internal application of a driving current to create an electric field between two electrodes. Top and side view diagrams of the sample holder can be seen in Figures 2.4 and 2.5 below.

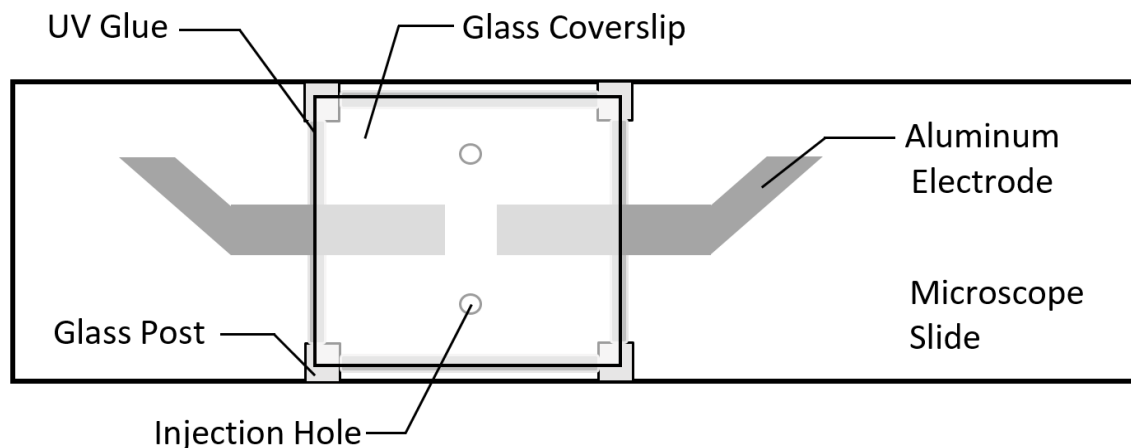


Figure 2.4: Top view of the complex sample holder used to study the charging and discharging characteristics of ADT-TES-F and PCBM in aqueous solution. The sample holder exhibits aluminum electrodes that allow the internal application of an electric field, allowing the study of the charging behaviors of coated microspheres.

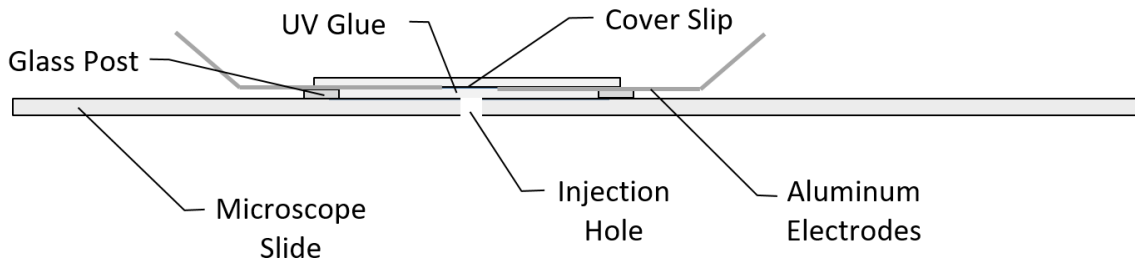


Figure 2.5: Side view of the complex sample holder used to study charging and discharging behaviors of ADT-TES-F coated microspheres and PCBM.

To prepare an electrode sample holder, two dots are marked on the microscope slide where holes will be drilled to allow the injection of a sample solution into the completed holder, see Figure 2.6 for hole placement. These holes are drilled with a diamond tipped dremel tool. After the holes are completed the slide is washed with toluene and rinsed with DI water in the fume hood, to ensure that all glass particles are removed from the glass surface. The presence of glass particulates in the sample holder's containment chamber would render the sample holder and experimental data collected from it unusable.

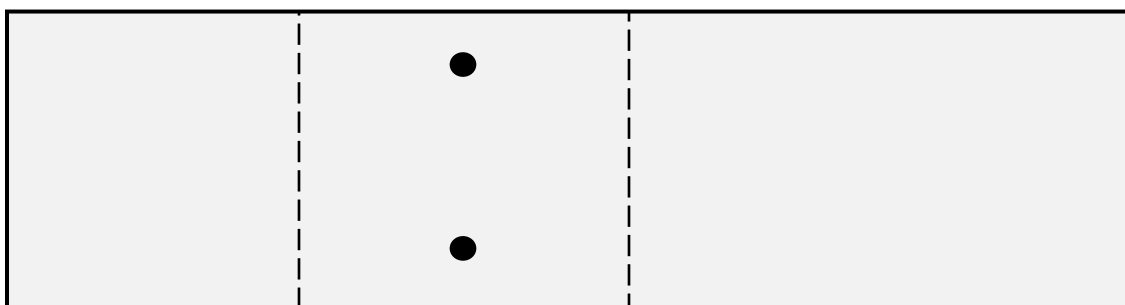


Figure 2.6: Locations for injection holes are marked in the center of the allowed space for the coverslip, separated enough to allow electrodes to be placed between them.

Four small squares are cut from a cover slip, each square approximately 5 mm on each side. Using UV glue, these squares are attached to the 4 corners of the dotted square in Figure 2.6 and the slide is placed above an ultraviolet lamp for 30 seconds to allow the glue to dry. The 4 squares will become the platforms to which the glass coverslip is attached. The slide is put aside on a sterile matt.

Two aluminum electrodes approximately half a centimeter wide and 6 cm long are cut from a strip of aluminum foil. The electrodes are then attached, dull side down, to the center of a coverslip with a 200-400  $\mu\text{m}$  gap between them. This gap will allow the aqueous sample solution to reside between the electrodes where the electric field is applied. The electrodes are attached to the coverslip with UV glue and allowed to dry over an ultraviolet light for 30-45 seconds. See Figure 2.7 for a descriptive diagram of how a coated microsphere will interact with the aluminum electrodes. The sphere is suspended inside the sample holders cavity between the electrodes attached to the glass coverslip. UV glue is placed on the 4 glass squares on the microscope slide and the coverslip with electrodes is placed, electrodes down, onto the 4 posts, see Figure 2.4. The holder is placed over the UV lamp for 30-45 seconds. Lastly, the edges of the coverslip are lined with UV glue, creating a sealed chamber that will house the sample solution. The

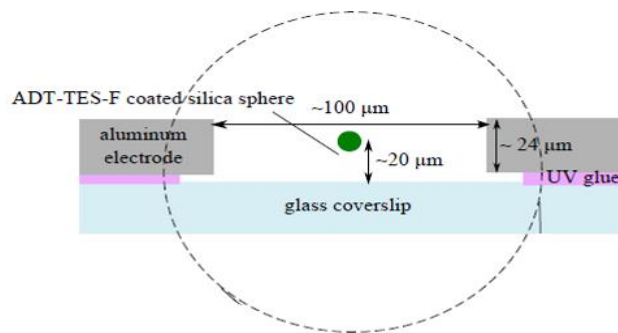


Figure 2.7: Position of the microsphere and aluminum electrodes in aqueous solution and the containing sample holder, Image courtesy of the Organic Photonics and Electronics lab.

finished holder is placed over the UV lamp for 60 seconds to ensure all UV glue is dried before the sample solution is injected through the holes drilled in the bottom of the slide. These sample holders, can be made in advance and stored for future use since the sample can be injected after the holder is complete.

## 2.4 Experimental Set-up

The optical tweezers set-up was constructed in Dr. David McIntyre's Optical research lab at Oregon State University. The set-up was transferred to The Organic Photonics and Electronics lab under Oksana Ostroverkhova by graduate student Mark Kendrick and maintained and rebuilt by Rebecca Grollman during her graduate work at Oregon State University. A basic overview schematic is shown in Figure 2.8 below.

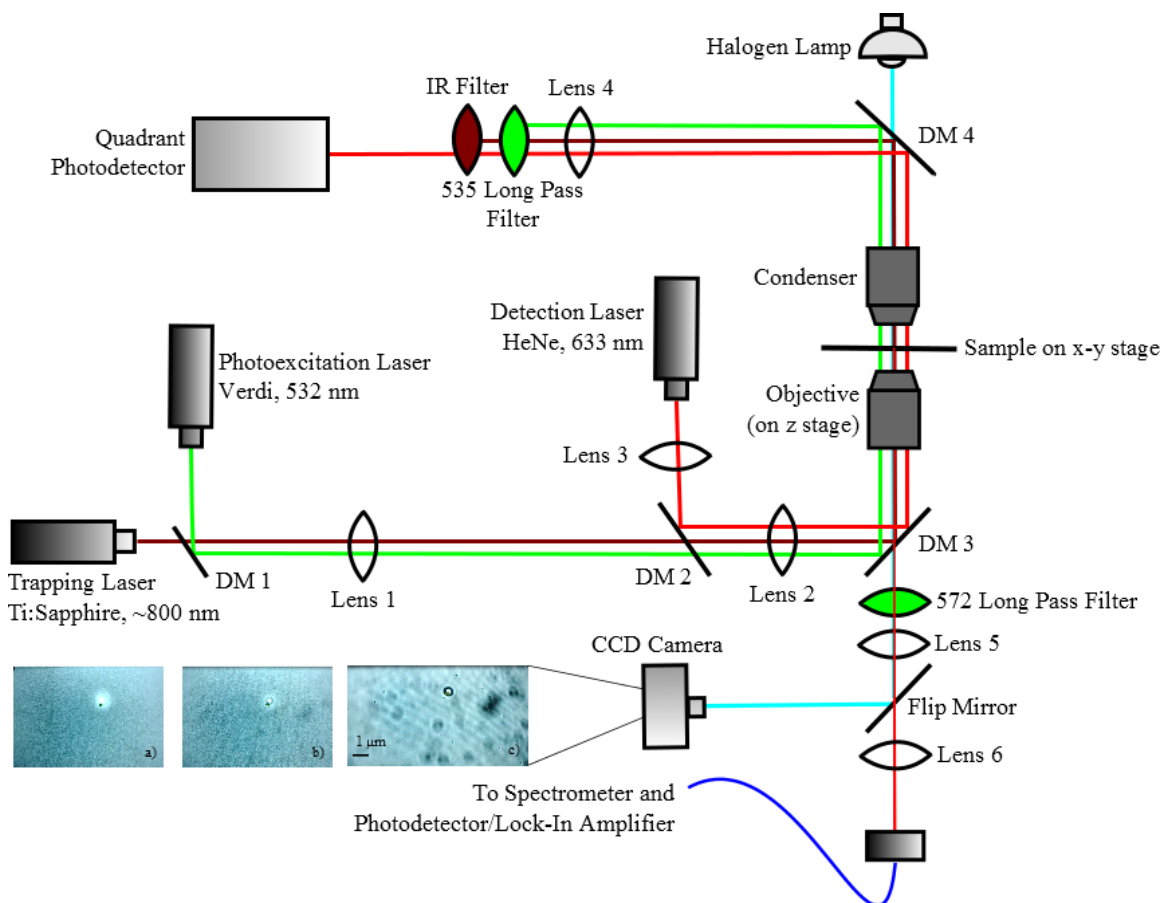


Figure 2.8: Optical trapping set-up from David McIntyre's optical research lab. Image courtesy of Rebecca Grollman of the Organic Photonics and Electronics Lab.

The trapping set up contains three lasers used for collecting the stiffness and charging data. The main optical trapping laser is an 800 nm Ti-sapphire laser. An infrared laser is used for trapping so it does not interact with the silica sphere or organic material by exciting electrons or inducing photo luminescence.

The Ti-sapphire laser is guided through a series of lenses and mirrors directing it to the objective and condenser shown in Figure 2.8. The focus of the trapping laser is placed inside the sample holder on the x-y stage by adjusting the separation between the objective and condenser. The photoexcitation laser is a 532nm Verdi-5. The Verdi induces photoluminescence and excites electrons in the organic materials. Lastly, the He-Ne (Helium-Neon) laser in conjunction with a QPD, monitors the position of the sphere trapped by the Ti-sapphire laser. Connected to the output of the QPD is a DAQ data acquisition unit and an oscilloscope, which collects and displays the QPD signal. This signal is used to calibrate the QPD's collected signal by repositioning lens 4 in Figure 2.8. Lens 4 is responsible for optimizing the signal observed on the oscilloscope and to calibrate the QPD.

A halogen lamp, above the condenser, is coupled with a CCD camera below and to the left of the stage. When the lamp is turned on an image of the trapped sphere and surrounding environment is displayed through the CCD camera onto a small monitor screen. This allows for the observation of microspheres and chunks of PCBM in solution at a microscopic level. Examples of the observed display can be seen in Figure 2.8 at the lower left. Various filters are placed throughout the set-up, these block the light of particular wavelengths that are not needed or could damage a specific piece of equipment. The QPD is protected by an IR filter to eliminate the trapping laser and a 535 nm long pass filter to eliminate the excitation laser. Both lasers are used at much too high an intensity for the QPD to handle, if the filters were not in place the QPD would suffer damage. The third filter, a 572 nm long pass, is placed before the CCD camera to allow only the trapping Ti-sapphire and He-Ne lasers through to the CCD. This filter can be removed during alignment procedures to help align the focal patterns of the three lasers.

Seen in the lower right corner of Figure 2.8, a spectrometer is attached at a 90 degree angle to the CCD camera and in the direct path of the lasers. This spectrometer is coupled with a SpectraSuite program to

capture the PL induced by the 532 nm excitation laser. The captured spectrum is caused by photoexcitation and subsequent relaxation with emission of a photon. This property can be used to clarify if a sphere is coated with ADT-TES-F or not. When a sphere is captured, the 532 nm laser is focused onto the sphere, all other lights are shut off and all lasers are filtered out, only allowing the light due to the photoexcitation to be fed to the spectrometer. If the sphere shows a spectrum with a peak around 500-600 nm and a glowing is seen on the CCD camera feed, then the sphere is known to be coated with active ADT-TES-F and data collection on the charging behaviors can be collected.

## 2.5 Data Collection

### 2.5.1 Trap Stiffness Measurements

A trap stiffness sample holder is constructed with 50  $\mu\text{L}$  of water and silica spheres, refer to section 2.3.1 for specifics on the process and methodology of sample holder construction. The completed sample is placed on the x-y stage of the optical trapping set-up, see Figure 2.8, "Sample on x-y stage". The CCD camera is turned on along with the 800 nm Ti-sapphire and the 633 nm He-Ne laser. The laser alignment is checked through the CCD camera feed and a sphere is brought into focus using the telescoping motion of the objective on a z-stage. Using the x-y stage, a sphere is brought to the center of the lasers' focal patterns where the sphere becomes trapped. The He-Ne shines onto the trapped sphere and the surrounding area, the QPD is turned on and attached to a DAQ board which is in turn attached to a computer with a DAQ connection card. A LabVIEW program is then used to collect 30 second bursts of the spheres Brownian positional data from the QPD. In the 30 seconds,  $2^{14}$  data samples are taken at a sampling rate of 10 kHz. This data is stored in simple two column text files that are run through a MATLAB program that analysis the positional data to produce the simulated trap stiffness of the optical tweezers. The program was written by Rebecca Grollman, see section 1.6 for more detail on MATLAB data analysis. This process is also used to understand the coupled behavior of trapping laser power and optical trapping stiffness. To test this, data is collected and analyzed at a variety of trapping laser powers and a plot is produced to show the linear correlation between laser power and trap stiffness.

### 2.5.2 Control Charge Measurements

100  $\mu\text{L}$  of ADT-TES-F, PCBM, or ADT-TES-F and PCBM solution is injected into an electrode sample holder's chamber. The filled sample holder is then placed onto the x-y stage of the optical trapping set-up. Two alligator clips are attached to the sample holder's aluminum electrodes and then connected to a function

generator that will apply the needed oscillating signal to induce an electric field between the electrodes. The trapping laser is turned on and the alignment checked by observing the focal pattern captured by the CCD camera. The He-Ne and Excitation laser are aligned with their focal patterns matching that of the trapping laser. Using the x-y stage, the sample holder's position is adjusted until a sphere is brought into view on CCD feed. The sphere is brought near the center of the trapping lasers focal pattern where it is held. All lights are turned off and a filter is placed blocking out the trapping laser's pattern. The excitation laser is turned on and allowed to shine onto the trapped microsphere. If the sphere is coated a glowing circle will appear on the camera feed where the sphere would be shown. Below in Figures 2.9 and 2.10, the CCD camera feed of a trapped microsphere with the trapping laser filtered out is shown along with the glowing behavior of a coated sphere.



Figure 2.9: Coated micro-sphere trapped in optical tweezers with trapping laser filtered out with IR filter. Feed from CCD camera displayed on viewing screen.

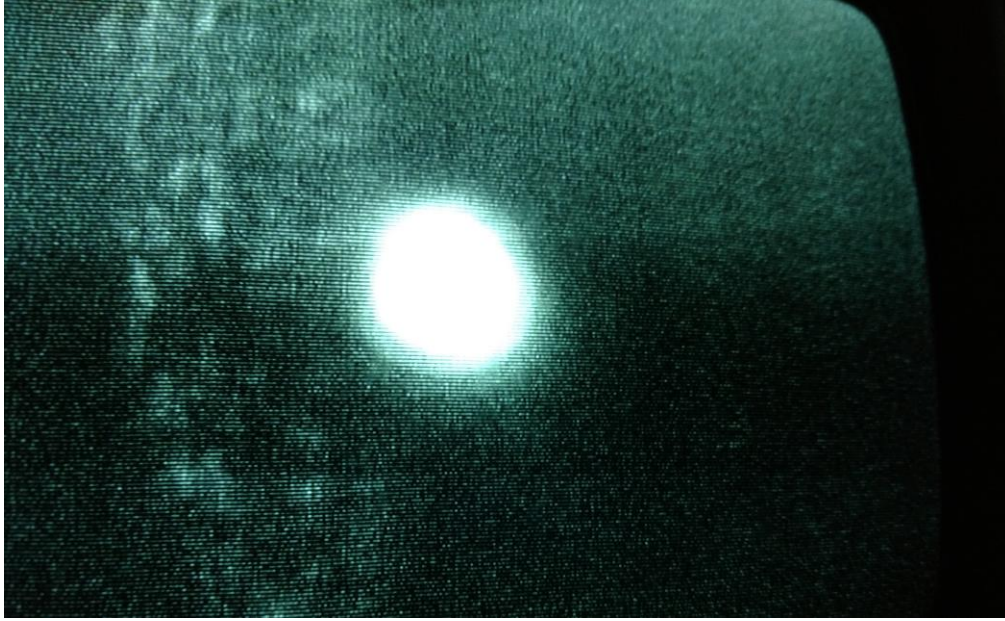


Figure 2.10: Coated microsphere reacting to the excitation laser. Observing photo luminescence caused by the excitation laser inducing electron transport which results in photons being released.

A signal is sent from the function generator to the aluminum electrodes, 5V magnitude and 100 Hz driving frequency. The oscilloscope is attached to the QPD to monitor the outgoing signal sent to the computer for data collection. If the signal is offset by an amount greater than 50 mV, the position of Lens 4, see top-center of Figure 2.8, is adjusted to realign the signals until they are centered. When the signals are aligned and within acceptable bounds, LabVIEW is used to collect 30 second bursts of data collection with and without the presence of the excitation laser. 262,144 samples are taken for each run at a 10kHz sampling rate. Collected data is output in a basic two column text file that will be fed to the trap stiffness MATLAB code used previously then the resulting information produced by the trap stiffness analysis is fed to a second MATLAB code written by Rebecca Grollman that produces the magnitude surface charge of the trapped sphere.

### 2.5.3 Charge as a function of Driving Frequency

The process described in section 2.5.2, is replicated in the process of testing the charge behavior as a function of the applied electric fields driving frequency. The driving field frequency, control set at 100 Hz, is varied from 10 Hz up to 10 kHz. A 30 second data run is taken at each step of the variance, stepping up by 10 Hz, 50 Hz, 100 Hz, or 200 Hz. Performing these measurements gives a spectrum of surface charges for the same microsphere. The resulting data and plots are used to understand the experimental role that the applied fields driving frequency plays and what the most accurate frequency for data collection is.

### 2.5.4 Charge as a Function of Driving Field Intensity

Similar to the driving electric field frequency, the driving electric field intensity is varied to understand the optimal signal magnitude to apply during data collection. The intensity of the field is changed by altering the peak to peak amplitude of the function generator's signal applied to the sample holder's aluminum electrodes. The driving signal amplitude is varied in a range from 100mV to the maximum peak-to-peak supported by the function generator of 10V. At each variance step a 30 second data run is collected, as previously expressed, the collection contains 262,144 data samples collected at a rate of 10kHz. The collected data is fed to both the trap stiffness MATLAB code and the surface charge code and used to better understand the roll that the field intensity plays in the process of studying the charging behavior of microspheres and coated microspheres.

### 2.5.5 Charge as a Function of Excitation Laser Intensity

Testing the varying effect of the excitation laser's intensity is controlled by a gradient disk placed in the path of the excitation laser's beam. The disks gradient gradually increases in transparency in a clockwise direction, rotating the disk to a more transparent location increases the excitation lasers intensity. An electrode sample holder is filled with one of the four testable solutions, shown in Figure 2.1 and explained

in section 2.2. The sample holder is then placed on the optical tweezers x-y stage and attached to the function generator. A coated or non-coated sphere is trapped using the 800nm Ti-Sapphire and the He-Ne laser is applied. A signal is applied across the sample holder's aluminum electrodes and the excitation laser is focused onto the trapped sphere. LabVIEW is used to record 30 second bursts of data at different laser intensities. Experiments with basic silica spheres and silica spheres with PCBM acceptor floating in solution are used to understand the control behavior of silica interacting with the excitation laser. This information will be applied to the numbers collected during the experimental testing of spheres coated in ADT-TES-F with and without PCBM suspended in solution to account for the control behavior of plain silica interacting with the 532 nm excitation laser.

## Chapter 3: Results and Discussion

The end goal of these experimental methods is to study the charging and discharging behaviors of ADT-TES-F and PCBM as an organic charge transfer pair. Most opto-electronic applications of organics rely on donor acceptor combinations. The acceptor provides low energy levels for electrons from the donor molecule to transfer to, encouraging charge motion produced by a decrease in energy level. In order to accurately analyze the surface charging behavior, proper experimental parameters must be implemented. The trapping laser power and trap stiffness correlation must be analyzed to understand the trending behavior between them. The trapping power is set at a reasonable level to hold the sphere but not restrict the particle's motion to a point of corrupting the positional data collected by the QPD.

The correlation between the surface charge density data and applied electric field parameters, such as field frequency and magnitude, are studied to ensure the clarity and accuracy of the collected and analyzed data. An electric field must be applied that induces enough particle oscillation for the MATLAB program to output a constant and reliable value for the surface charge density of the microsphere and ADT-TES-F coating. Additionally, the effect of an excitation laser on the surface charge density value of a non-coated sphere is observed to understand the induced charge behavior.

## 3.1 Trap Stiffness

### 3.1.1 Stiffness as a Function of Trapping Laser Power

Plain silica spheres in Milli-Q filtered water were tested to observe the correlation between trapping laser power and the simulated trap stiffness of the optical trap. No electric field is applied for this experiment.

Figure 3.1 below shows the approximate linear behavior between the optical trapping constant and the trapping laser power.

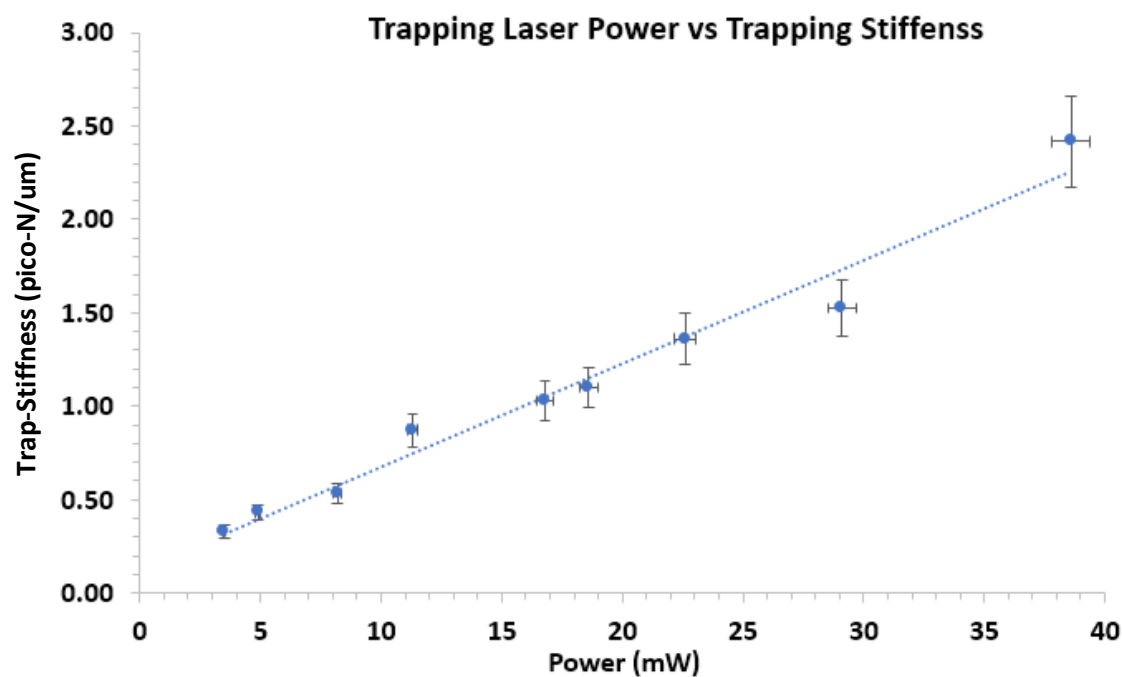


Figure 3.1: Linear behavioral relation between trap stiffness constant and the trapping laser power. Data collected from multiple runs at each power on the same sphere. Error bars display a hard set 10% value of error, this accounts for standard deviation for each averaged point.

The linear behavior shown in Figure 3.1 allows the trapping laser power to be adjusted with the knowledge of how the trap stiffness will change and what the expected stiffness will be. From the collected data it is known that as the trapping laser power increases the trap stiffness will linearly increase. This allows the prediction of how the spheres motion will be gradually restricted as the laser power is adjusted in future experiments. When the sphere is used to study charging and discharging behaviors, the induced oscillation

from the applied electric field will be cut off if the trap stiffness is too high. A higher laser power, inducing a higher trap stiffness, will cause the spheres motion to be restricted and the positional data collected to be corrupted. Using the linear behavior from the data in Figure 3.3, the adjustment of laser power can be made to find a desired trap stiffness that will not constrain the spheres induced oscillation.

## 3.2 Surface Charge of Microsphere

### 3.2.1 Silica in Water

Silica spheres in a solution of Milli-Q filtered water were tested to show plain silica's charging behaviors under varying conditions. This helps predict the continuing behaviors that will be seen and built upon during the three progressive experiments shown in Figure 2.1. The first parameter tested was the surface charge variance of a plain silica sphere in Milli-Q water as the driving fields frequency is altered. Past researchers working on this project used a driving field frequency of approximately 100 Hz while collecting surface charge data for coated and non-coated microspheres. The data displayed in Figure 3.2 shows that

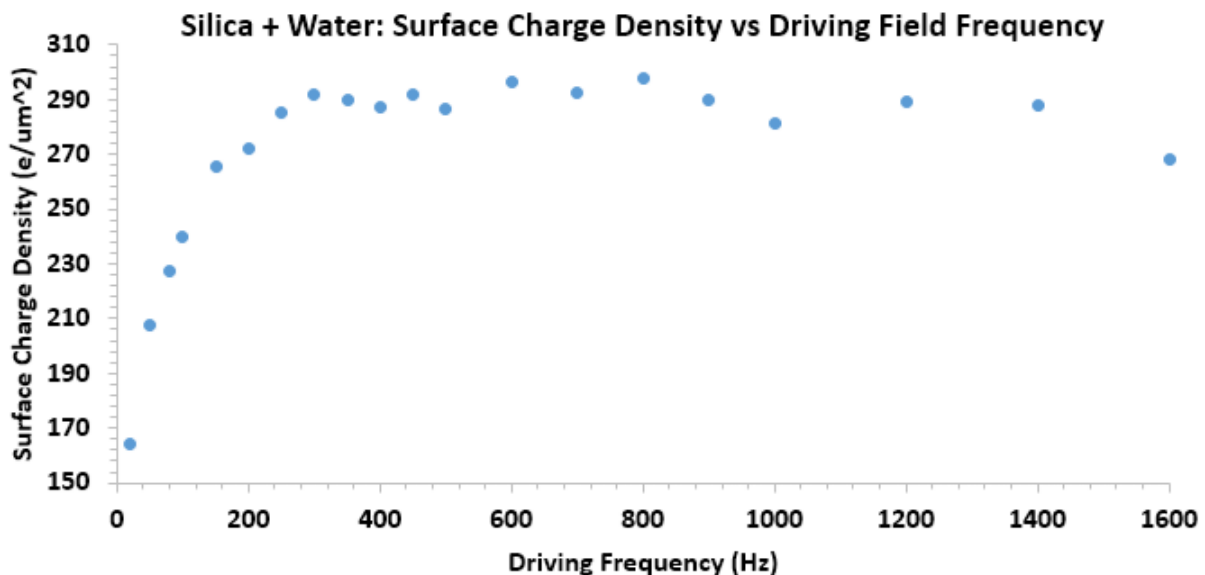


Figure 3.2: Surface charge density behavior of a silica microsphere as a function in a spectrum of driving field frequencies. After the mark of 300 Hz the charge behavior becomes constant. The electric field intensity is set to approximately 2200 V/m.

a driving field below 300 Hz yields an approximate 15% lower charge value than that of higher frequencies.

At approximately 300 Hz the charge behavior of the microsphere displays a constant behavior. A constant surface charge is best obtained in a frequency range that displays a constant trend in the surface charge density readings. Further experimentation will be conducted using a driving field of approximately 400 Hz, a frequency inside the spectrum of constant behavior. Increasing the field frequency induces a characteristic oscillation that can be accurately analyzed by the MATLAB code. The higher the field, to an extent, the more reliable the magnitude of the surface charge and the more accurate the surface charge density.

The testing of plain silica in Milli-Q continued to observe the surface charge behavior when the 532 nm excitation laser is applied and when the field intensity is varied by adjusting the peak to peak voltage of the driving signal from the function generator. The excitation laser should not show any significant effect when shown on a plain silica sphere. The silica material is not charge interactive with a low power 532 nm laser; therefore, the surface charge should not vary with the excitation lasers presence.

The experimental data proves the theory correct. Figure 3.3 shows a distinct lack of correlation between surface charge, or surface charge density and the presence of an excitation laser at varying powers.

There will be no background effect present in the charge variation of the coated microspheres when exposed to a 532 nm excitation laser used to induce charge transfer and photoluminescence.

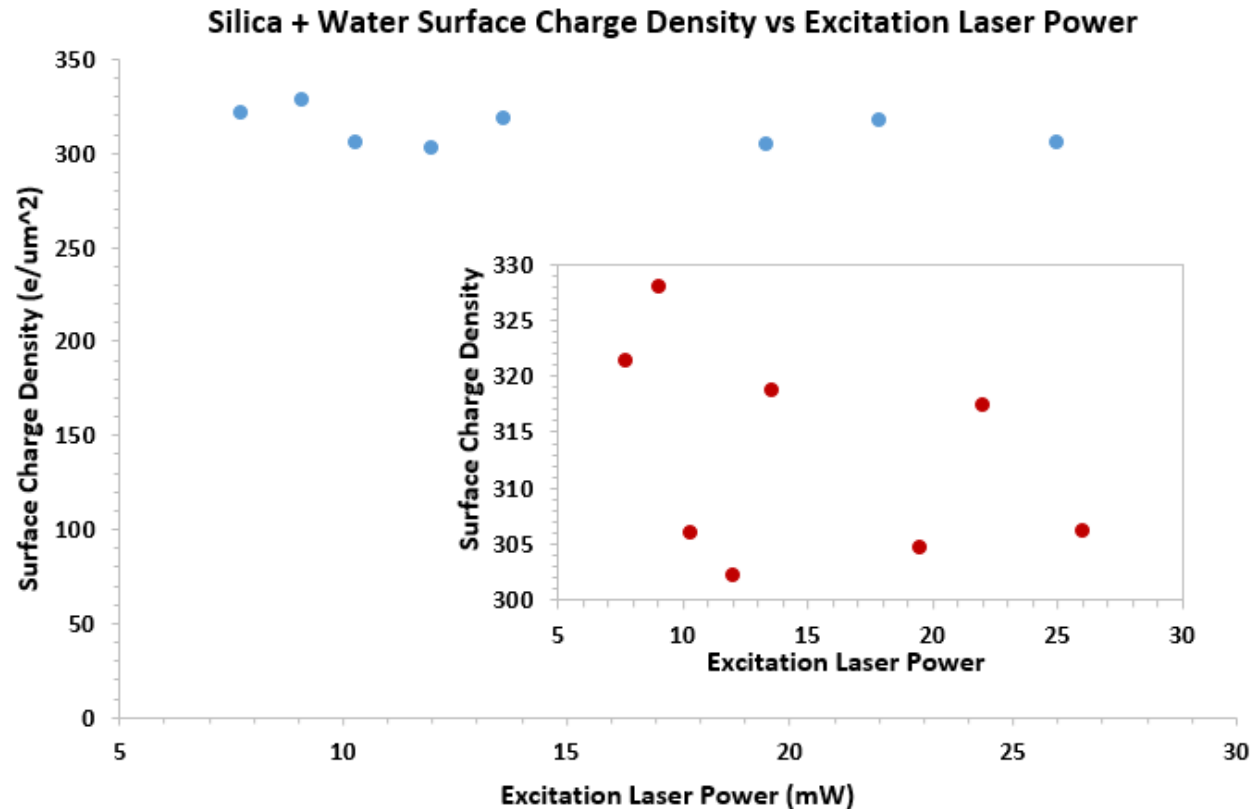


Figure 3.3: Surface charge variance with a spectrum of laser power intensities for the applied 532 nm excitation laser. The 10% variations seen in this plot are standard between data runs, they show no relation to the excitation laser. The electric field intensity is set to approximately 2600 V/m and the frequency is set to 400 Hz.

The lack of effect shown by the excitation laser is due to the substantial band gap present in the silica sphere and the absence of reactive behavior with the 532 nm laser, specifically chosen to induce PL in the ADT-TES-F coating that will be used in future experiments.

The last experimental parameter that is tested for plain silica in a Milli-Q suspension is the varying magnitude of the applied electric field that allows for the measurement of the spheres surface charge.

If the field is too strong it will cause the sphere to oscillate at a large amplitude and force the sphere out of the optical trap. The amplitude of the field must be high enough to accurately measure the magnitude of the surface charge of the sphere. The surface charge is calculated by analyzing the extent to which the electric field influences the motion of the particle. If the field is too weak the particle will not be affected to a measurable amount, this will render an incorrect surface charge value. Figure 3.4 displays the behavior of the silica spheres surface charge density as the magnitude of the electric field is adjusted. The ideal field is shown to be greater than 2500 V/m where the measured surface charge levels to a reasonable constant level.

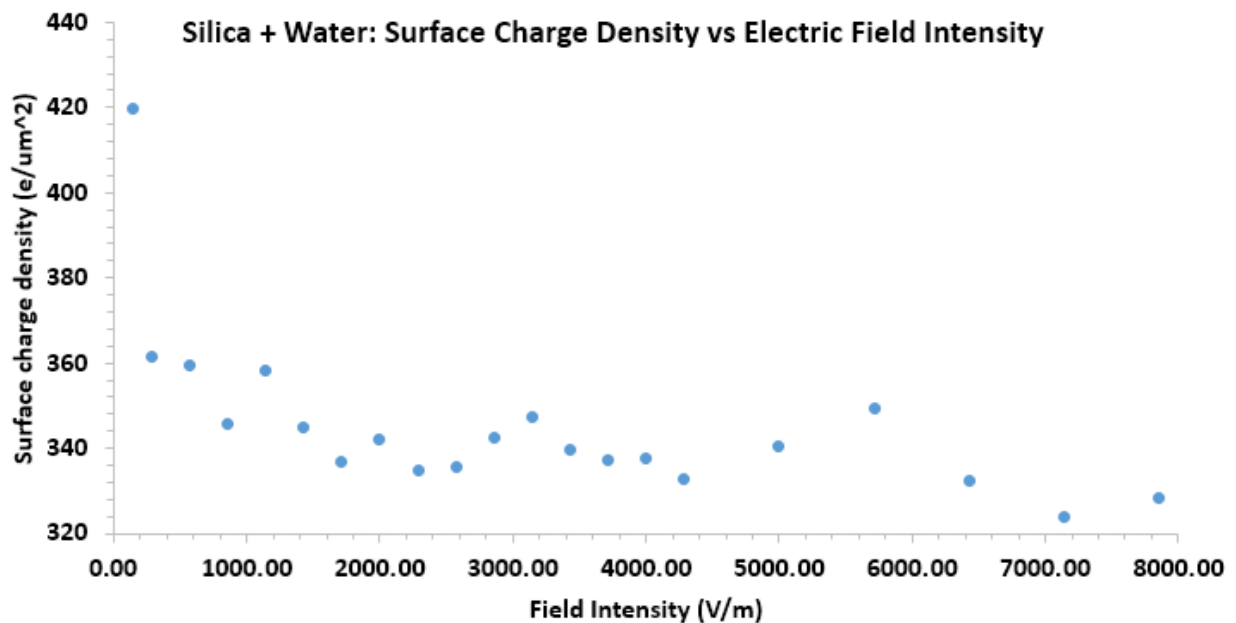


Figure 3.4: Surface charge of a microsphere as a function induced electric field's magnitude between the aluminum electrodes. Constant behavior is observed after an electric field magnitude of 2000 V/m. This will be the trusted region on future experimentation. The electric field frequency is set to 400 Hz.

Two different methods obtain the needed field strength. The distance between the electrodes in the sample holder can be adjusted or the amplitude of the driving field can be adjusted by changing the peak to peak voltage of the function generators supplied signal. In the end, both methods of adjustment are required to reach the desired field strength. A sample holder is made with an approximate width between the electrodes and then a signal amplitude is chosen that provides the appropriate electric field. The field is found using the simplistic capacitor field equation shown by equation (6).

$$E_c = \frac{V_{P-P}}{D} \quad (6)$$

where  $E_c$  is the electric field stored in a capacitor, between the two electrodes in this case,  $V_{P-P}$  is the peak to peak voltage of the applied driving signal, and  $D$  is the distance between the electrodes, representing the plates of the capacitor.

### 3.2.2 Silica in Water with PCBM

The same three parameters tested for the plain silica spheres in Milli-Q water were tested for the sample solution of silica spheres in Milli-Q water with PCBM suspended in solution. The surface charge density behavior was tested as a function of frequency. The addition of PCBM did not result in a significant behavior change in the surface charge density as a function of driving field frequency. The difference in surface charge density magnitude displayed in the data is common from sphere to sphere, it does not correlate to the presence of PCBM in solution.

Similar to the charge behavior in the basic silica and water solution, see Figure 3.2, the surface charge density as a function of frequency displays a constant behavior past the 300 Hz mark. Compounding on previous results, the ideal driving frequency is still within the region of 300-1000 Hz, the chosen 400 Hz driving field frequency will be implemented in the final experiments seen in Figure 2.1 section 4. This driving frequency will ensure that reliable surface charge measurements are collected and analyzed

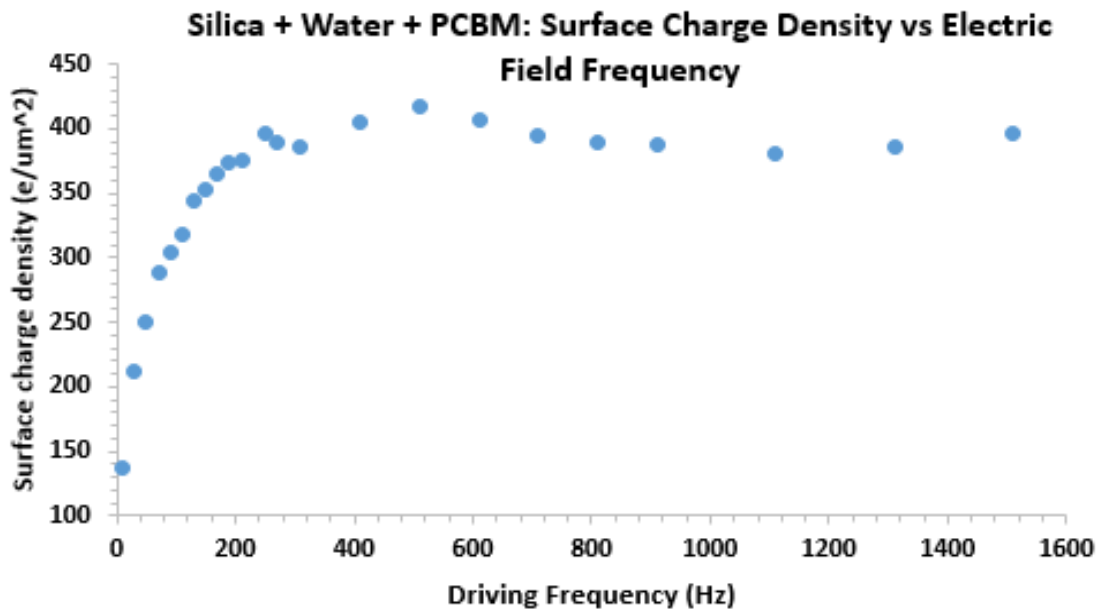


Figure 3.5: Surface charge density correlated to the driving field frequency. Similar behavior as the Silica and water is shown depicting a more linear region of behavior past the 300 Hz mark. The electric field intensity is set to approximately 2800 V/m.

The theory behind the behavior displayed in Figure 3.4 above is identical to that previously stated for Figure 3.2. The higher end of the frequency spectrum denotes a higher energy field, the higher energy field interacts significantly with magnitude of surface charges on the silica sphere, giving a proper measurement.

Similar to the behavior seen in Figure 3.3, the surface charge density behavior as a function of excitation laser power, the presence of the 532 nm excitation laser shows no direct effect on the surface charge density of a non-coated silica sphere with PCBM suspended in solution with it, Figure 3.6. The electron acceptor does not notably encourage charge transfer or excitation in the plain silica sphere. Similar to the silica and water test, the lack of effect is due to the non-reactive nature of silica with the 532 nm laser and the 1.1 eV HOMO LUMO gap that the laser is not powerful enough to cause an electron to excite through.

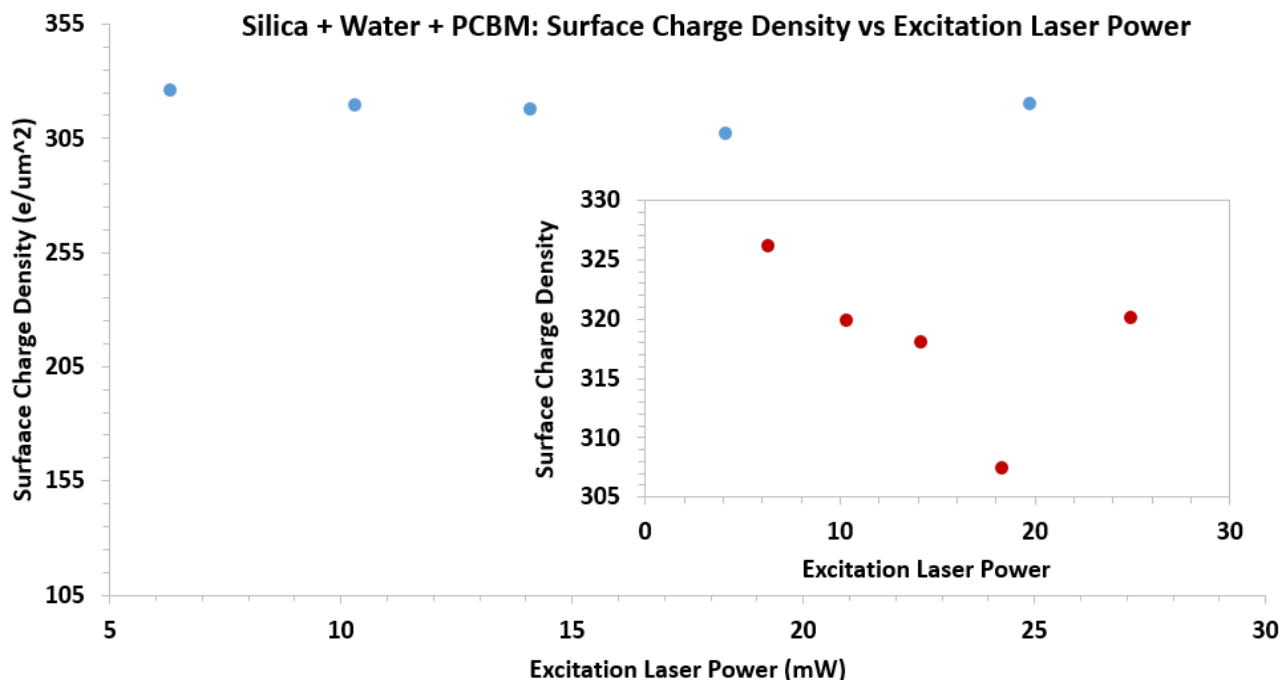


Figure 3.6: Surface charge density does not change with laser power. There will be no ambient change transfer effect when testing spheres coated in a donor molecule, ADT-TES-F. The 10% drift between charge measurements is a normal fluctuation between data readings, it does not correlate to the excitation laser. The electric field intensity is set to approximately 2500 V/m and the frequency is set to 400 Hz.

In future experimentation on coated spheres with and without PCBM suspended in solution, it is expected that the excitation laser will only cause electron excitation and PL in the ADT-TES-F coating, no ambient electron counts or excitations will be present due to the silica sphere and PCBM suspension.

The final parameter tested to ensure the accurate collected of surface charge density data for spheres coated in ADT-TES-F, observing the correlation between surface charge density and the driving field intensity of silica spheres in water with PCBM suspended in solution, Figure 3.7. Similar to the behavior observed in the silica and water control testing, the field intensity shows a downward trend initially then adopts a linear trend at a lower surface charge density. The field must be strong enough to fully interact with the magnitude of the charge on the spheres surface. These three control tests conducted on the silica in water solution with PCBM show that the presence of PCBM does not affect the control behavior of silica. PCBM will only help induce charge transfer and charging behaviors in the presence of the chosen donor molecule ADT-TES-F.

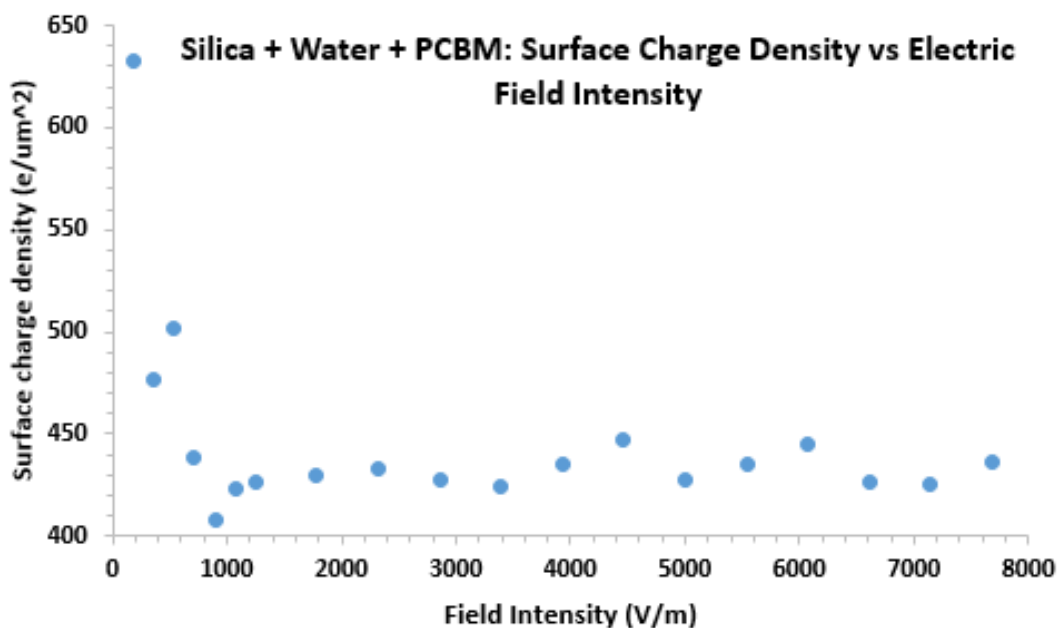


Figure 3.7: Surface charge density becomes reasonably linear after the 1000 V/m mark. A field stronger than 2000 V/m will accurately produce surface charge density values. The electric field frequency is set to 400 Hz.

Supplying the proper parameters to the final experiment, studying the charging and discharging behaviors of silica microspheres coated in ADT-TES-F donor with PCBM acceptor suspended in solution, is exceedingly important to acquire an accurate measure of the surface charge density and the charging and discharging behaviors of the organic semiconductors.

## Chapter 4: Conclusions

Using the highly sensitive non-contact method of surface charge measurement, we measured the charging behavior of plain silica spheres and silica spheres paired with PCBM. Varying conditions were applied to fully understand the charging behaviors. The driving electric field was found to be most accurate at producing reliable surface charge density values when the fields frequency was set to greater than 400 Hz and when the field intensity was set to 2000-2500 V/m. In previous research the electric field frequency and amplitude were set to values that did not yield a reliable surface charge. The electric field applied to the coated or noncoated spheres must exhibit a driving frequency greater than 300 Hz in contrast to the previously used 100-110 Hz. The electric field amplitude must be greater than 2000 V/m to produce reliable surface charge measurement in contrast to the previously used 500-1000 V/m field. The power of that excitation laser has no effect on the surface charge density of plain silica spheres regardless of the presence of PCBM. Knowing the required parameters removes the need to have a calibration factor applied to future experiments conducted with spheres coated with the photo luminescent ADT-TES-F. These frequency and intensity requirements for this experiment are likely due to Roberts's method of MATLAB coding used to analyze the collected data rather than them altering the surface charge of the sphere. Until a different analysis method is used, all future study of ADT-TES-F and PCBM will use the experimental parameters found to be ideal from these results; a driving field intensity of 2000 V/m or greater and a driving field frequency of 400 Hz or greater.

## Acknowledgements

Special thanks go to my advisor and mentor, Oksana Ostroverkhova for her guidance and patience during my time of research practice at Oregon State University. I would like to thank my research partner Rick Wallace for his consistent effort in the pursuit of scientific knowledge and his immense MATLAB coding efforts. Also, I would like to thank Rebecca Grollman, for her direction and energetic assistance during my time in the Organic Photonics and Electronics lab. My research efforts would have been for not had she not been a constant source of intuition and scientific knowhow.

This project was funded in part by the Undergraduate Research, Innovation, Scholarship, and Creativity (URISC) grant program at Oregon State University.

## References

- [1] Boxall, Andy . "The Galaxy S8 is exciting, but Samsung's rumored bendable phone sounds amazing." *Digital Trends*. N.p., 07 June 2016. Web. <<http://www.digitaltrends.com/mobile/samsung-project-valley-flexible-phone-launch-2017/>>.
- [2] Henriques, Afonso. "4D AMOLED Presentation." *Scribd*. Scribd, n.d. Web. 06 Feb. 2017. <<https://www.scribd.com/document/42669045/4D-AMOLED-Presentation>>.
- [3] Lin, Chih-Lung; Chen, Yung-Chih. "A Novel LTPS-TFT Pixel Circuit Compensating for TFT Threshold-Voltage Shift and OLED Degradation for AMOLED". *IEEE Electron Device Letters*. **28**: 129. [doi:10.1109/LED.2006.889523](https://doi.org/10.1109/LED.2006.889523).
- [4] F. Beunis, F. Strubbe, K. Neyts, and D. Petrov. Beyond millikan: The dynamics of charging events on individual colloidal particles. *Phys. Rev. Lett.*, **108**, 2012.
- [5] G. S. Roberts, T. A. Wood, W. J. Frith, and P. Bartlett. Direct measurement of the effective charge in nonpolar suspensions by optical tracking of single particles. *J. Chem. Phys.*, **126**:15, 2007.
- [6] R. R. Grollman, K. Peters, and O. Ostroverkhova. Surface charge measurements and (dis)charging dynamics of organic semiconductors in various media using optical tweezers. *Proc. SPIE, Organic Photonic Materials and Devices XVI*, 8983, 2014.
- [7] Lang, Matthew J., and Steven M. Block. "Resource Letter: LBOT-1: Laser-based optical tweezers." *American journal of physics*. U.S. National Library of Medicine, Mar. 2003. Web. 06 Feb. 2017. <<https://www.ncbi.nlm.nih.gov/pmc/articles/PMC1564163/>>.
- [8] J. W. Shaevitz. A practical guide to optical trapping. University of California at Berkeley, (Unpublished):19, 2006.
- [9] Paudel, Keshab, Brian Johnson, and Mattson Thieme. "Enhanced charge photogeneration promoted by crystallinity in small-molecule donor-acceptor bulk heterojunctions: Applied Physics Letters: Vol 105, No 4." *Enhanced charge photogeneration promoted by crystallinity in small-molecule donor-acceptor bulk heterojunctions: Applied Physics Letters: Vol 105, No 4*. AIP Applied Physics Letters, July 2014. Web. 06 Feb. 2017. <<http://aip.scitation.org/doi/10.1063/1.4891758>>.
- [10] K. R. Rajesh, K. Paudel, B. Johnson, R. Hallani, J. E. Anthony, and O. Ostroverkhova, "Design of organic ternary blends and small-molecule bulk heterojunctions: photophysical considerations". *Journal of Photonics for Energy* **5**, 057208 (2015).
- [11] Platt, A. D., M. J. Kendrick, M. Loth, J. E. Anthony, and O. Ostroverkhova. "Temperature dependence of exciton and charge carrier dynamics in organic thin films." *Physical Review B* **84**.23 (2011): n. pag. *APS Physics*. Web. <<http://journals.aps.org/prb/abstract/10.1103/PhysRevB.84.235209>>.

- [12] Kendrick, M. J., A. Neunzert, M. M. Payne, B. Purushothaman, B. D. Rose, J. E. Anthony, M. M. Haley, and O. Ostroverkhova. "Formation of the Donor–Acceptor Charge-Transfer Exciton and Its Contribution to Charge Photogeneration and Recombination in Small-Molecule Bulk Heterojunctions." *The Journal of Physical Chemistry C* 116.34 (2012): 18108-8116. ACS Publications. Web. <<http://pubs.acs.org/doi/abs/10.1021/jp305913s>>.
- [13] Mamada, Masashi, Hiroshi Katagiri, Makoto Mizukami, Kota Honda, Tsukuru Minamiki, Ryo Teraoka, Taisuke Uemura, and Shizuo Tokito. "Syn-/anti-Anthradithiophene Derivative Isomer Effects on Semiconducting Properties." *ACS Applied Materials & Interfaces* 5.19 (2013): 9670-677. ACS Publications. Web. <<http://pubs.acs.org/doi/abs/10.1021/am4027136>>.
- [14] Hummelen, Jan C., Brian W. Knight, F. Lepeq, Fred Wudl, Jie Yao, and Charles L. Wilkins. "Preparation and Characterization of Fulleroid and Methanofullerene Derivatives." *The Journal of Organic Chemistry* 60.3 (1995): 532-38. ACS Publications. Web. <<http://pubs.acs.org/doi/abs/10.1021/jo00108a012>>.
- [15] Dang M T, Hirsch L, Wantz G. *Adv Mater.* 2011;23:3597–3602. doi: 10.1002/adma.201100792. Web. < <https://www.ncbi.nlm.nih.gov/pubmed/21936074>>.
- [16] R. R. Grollman, K. Peters, and O. Ostroverkhova. Surface charge measurements and (dis)charging dynamics of organic semiconductors in various media using optical tweezers. *Proc. SPIE, Organic Photonic Materials and Devices XVI*, 8983, 2014.